Supporting information

Tunable Biomimetic Hydrogels from Silk Fibroin and Nanocellulose

Pramod Dorishetty,[a] Rajkamal Balu,[a] Sandya S. Athukoralalage,[a] Tamar L. Greaves,[b] Jitendra Mata,[c] Liliana de Campo,[c] Nabanita Saha,[d] Andrew C. W. Zannettino,[e] Naba K. Dutta*[,a,f] and Namita Roy Choudhury*[,a,f]

[a] School of Engineering, RMIT University, Swanston street, Melbourne, Victoria 3000, Australia.

[b] School of Science, RMIT University, Bowen street, Melbourne, Victoria 3000, Australia

[c] Australian Centre for Neutron Scattering, Australian Nuclear Science and Technology Organisation, New Illawarra Road, Lucas Heights, New South Wales 2234, Australia

[d] Centre of Polymer Systems, Tomas Bata University in Zlin, Nam. T. G. Masaryka 5555, 76001 Zlin, Czech Republic

[e] Faculty of Health and Medical Sciences, The University of Adelaide, North Terrace, Adelaide, SA, 5005, Australia

[f] School of Chemical Engineering and Advanced Materials, The University of Adelaide, North Terrace, Adelaide, SA, 5005, Australia

Corresponding Authors E-mail:

namita.choudhury@rmit.edu.au (N.R.C.).

naba.dutta@rmit.edu.au (N.K.D.).

Total number of pages : 8

Total number of figures : 6

Total number of tables : 2

TEXT

X-ray diffraction (XRD) analysis of the different types of nanocellulose used:

Figure S1 (A) shows the XRD pattern of cellulose nanocrystals (CNC), cellulose nanofibers (CNF) and bacterial nanocellulose (BC). The cellulose I characteristics peaks were observed at 2θ = 15.0°, 16.5°, 20.5° and 22.5°, which corresponds to planes ($1\bar{1}0$), (110), (102) and (200), respectively. Conversely, the cellulose II characteristics peaks were observed at 2θ = 12.5° and 20.0°, which corresponds to planes ($1\bar{1}0$) and (110), respectively.[1] Cellulose I, which is the native form of cellulose has the highest axial elastic modulus, whereas cellulose II is generally formed by regeneration.[2] The XRD data of CNC was deconvoluted with Gaussian curve fitting (Figure S1 (B)) using the MagicPlot software. The above 2θ values and an additional 2θ peak at 18.0° (amorphous contribution)[3] were used for the deconvolution.

Small angle neutron scattering (SANS) analysis of nanocellulose dispersions:

The SANS curves (Figure S2 (A)) of CNC, CNF and BC dispersions in D_2O showed three distinctive regions: a high-*q* Porod region, a mid-*q* Guinier region, and a low-*q* Porod-like region, which can also be clearly seen from Kratky plot (Figure S2 (B)). The high-*q* Porod slope of 3.0, 2.8 and 2.5 obtained (using power law fit) for CNC, CNF and BC can be attributed to the concentration fluctuations in nanocellulose fibrils or ribbons; where lower the slope value higher the fluctuations.[4] The mean inter-particle distance (d) of CNC in dispersion was estimated as ~67.0 nm from the correlation peak value using the relation $d = 2\pi/q$.[5] However, the SANS data of CNC dispersion could not be fit with a simple rigid rod model, considering the polydispersity of the system. Instead, the parallelepiped model with three characteristic dimensions: particle length, thickness and width were considered suitable based on literature reports.[6] The parallelepiped model fit to SANS data of CNC is shown in Figure S2 (C). On the other hand, the SANS data of CNF and BC were fit (at mid-*q* to high-*q*) with the flexible cylinder model – B(q) for intrinsic structure, and the power law function – A(q) for aggregation or network or entanglements at low-*q*, as shown in Figure S2 (D) and Figure S2 (E).[7] The combined form factor model function used for CNF and BC SANS data fitting is given in equation S1:

$$I(q) = A(q) + B(q) \qquad \text{(S1)}$$

where I(q) is the overall intensity of scattering. The length of the flexible cylinders was considered infinitively long for the fit based on atomic force microscopy results and the

observed trend of scattering (increasing intensity) towards low-*q*. The obtained data fit model parameters were used for deconvolution of regenerated silk fibroin (RSF)/nanocellulose composite hydrogel SANS data.

FIGURES

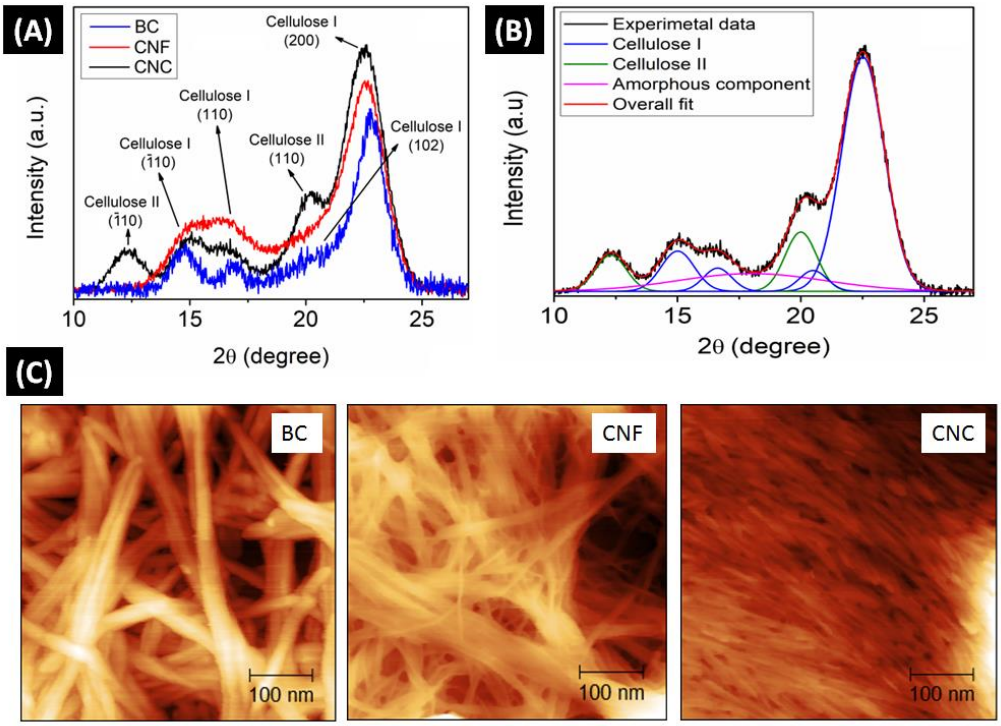

Figure S1. (A) XRD pattern of nanocelluloses. (B) Deconvoluted X-ray diffractogram of CNC. (C) AFM images of nanocelluloses.

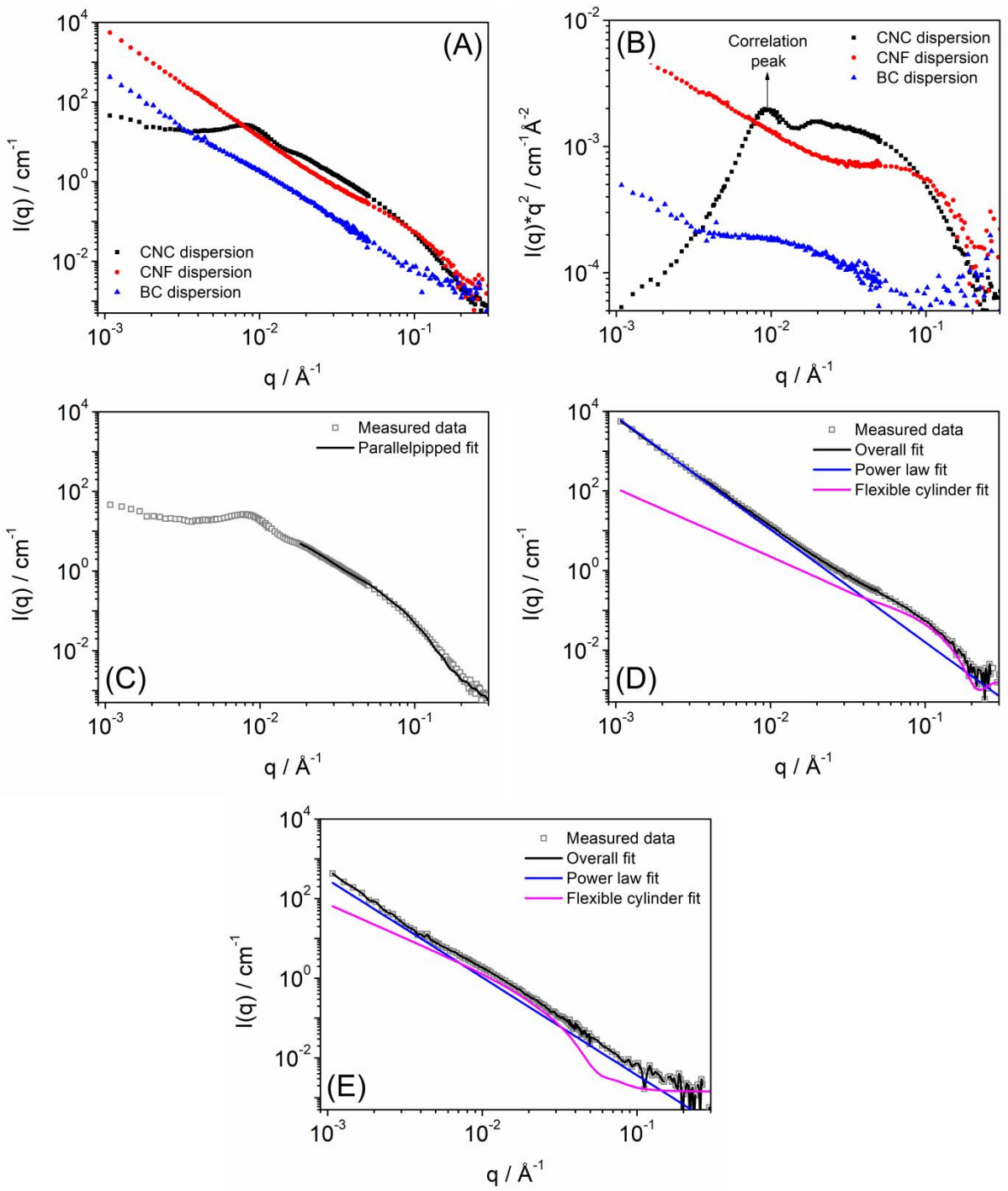

Figure S2. (A) SANS intensity profile and (B) Kratky plot of nanocellulose dispersion in D_2O. (C) to (E) are selective model function fits to the respective SANS data.

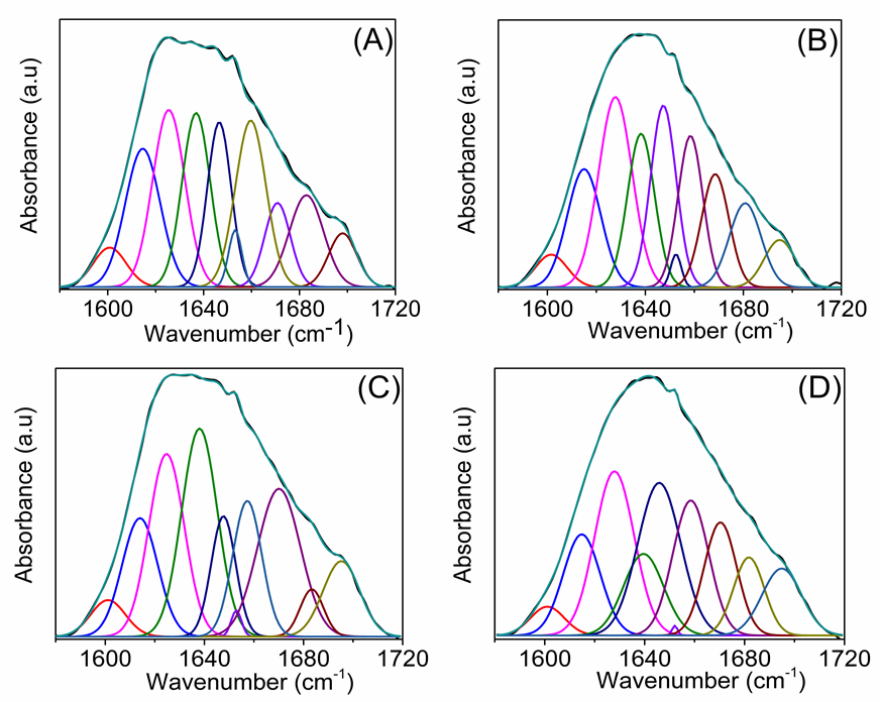

Figure S3. Deconvoluted FTIR spectra of (A) pristine regenerated silk fibroin (RSF), (B) RSF/CNC composite, (C) RSF/CNF composite and (D) RSF/BC composite hydrogels.

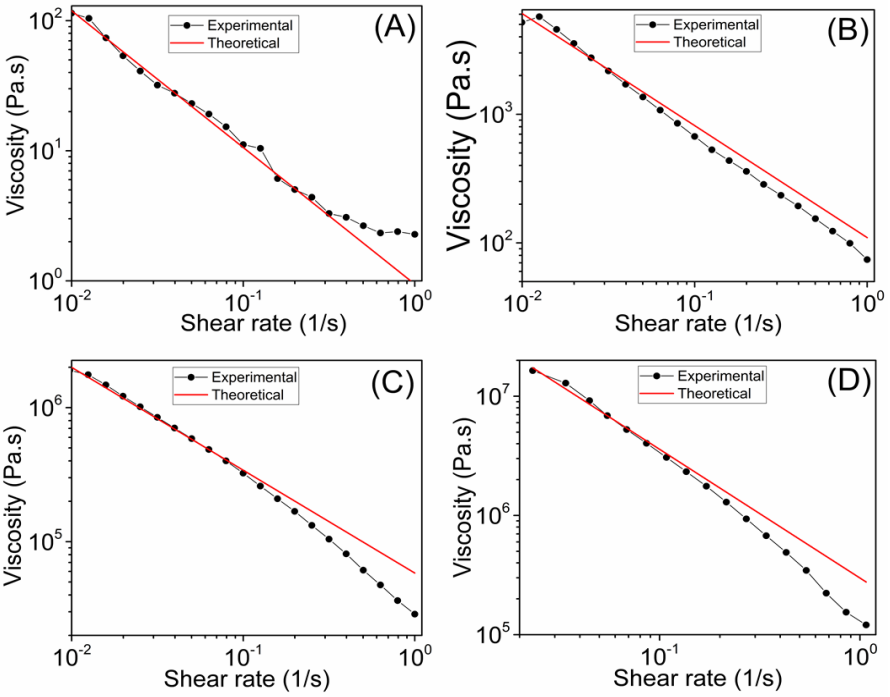

Figure S4. Experimental and theoretical (power law) fit of viscosity versus shear rate data of (A) pristine RSF, (B) RSF/CNC composite, (C) RSF/CNF composite and (D) RSF/BC composite inks.

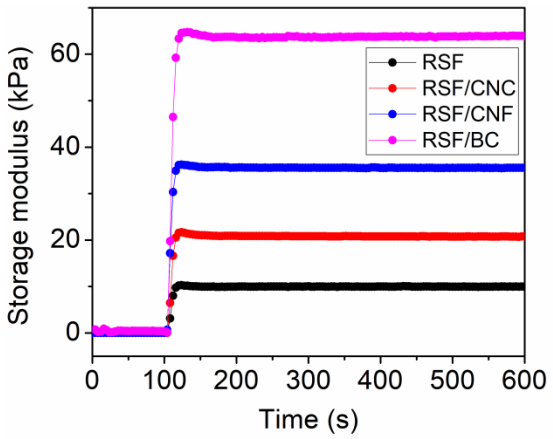

Figure S5. Dynamic oscillatory photocuring rheology showing crosslinking reaction kinetics of pristine RSF and RSF/nanocellulose composite inks. The lamp was turned on at 100 sec.

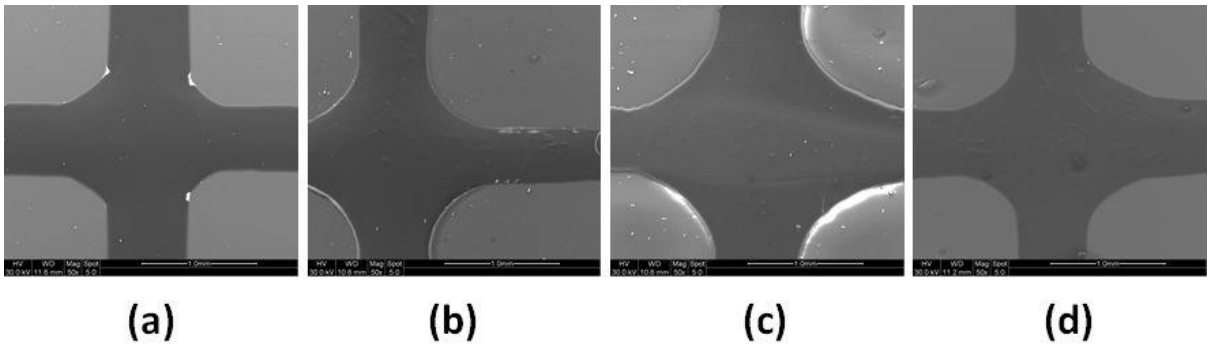

Figure S6. SEM micrographs (scale bar – 1 mm) of 3D printed and equilibrium water swollen hydrogels; where (a) is pristine RSF, (b) is RSF/CNC composite, (c) is RSF/CNF composite and (d) is RSF/BC composite hydrogels.

TABLES

Table S1. Estimated flow parameters of pristine RSF and RSF/nanocellulose composite inks.

Sample	K	n	R^2
RSF	0.94	0.05	0.99
RSF/CNC	109.92	0.12	0.96
RSF/CNF	4895.05	0.23	0.99
RSF/BC	182073.72	0.34	0.98

Table S2. Overall order of the properties of fabricated biomimetic hydrogel systems.

Property	Sample order
Inter-hydrophobic domain distance	RSF > RSF/BC > RSF/CNF > RSF/CNC
Water uptake	
Shear storage modulus	RSF/BC > RSF/CNC > RSF/CNF > RSF
Young's Modulus	
Tensile toughness	RSF/BC > RSF/CNF> RSF/CNC > RSF
Compression Modulus	
Energy dissipation	
Biocompatibility	RSF/CNF > RSF/BC > RSF > RSF/CNC
3D printability	RSF/CNC > RSF/BC > RSF > RSF/CFC

REFERENCES

(1) Novo, L. P.; Bras, J.; García, A.; Belgacem, N.; Curvelo, A. A. S., Subcritical Water: A Method for Green Production of Cellulose Nanocrystals. *ACS Sustainable Chem. Eng.* **2015,** *3*, 2839-2846.

(2) Moon, R. J.; Martini, A.; Nairn, J.; Simonsen, J.; Youngblood, J., Cellulose nanomaterials review: structure, properties and nanocomposites. *Chem. Soc. Rev.* **2011,** *40*, 3941-3994.

(3) Park, S.; Baker, J. O.; Himmel, M. E.; Parilla, P. A.; Johnson, D. K., Cellulose crystallinity index: measurement techniques and their impact on interpreting cellulase performance. *Biotechnol. Biofuels* **2010,** *3*, 10.

(4) Koizumi, S.; Yue, Z.; Tomita, Y.; Kondo, T.; Iwase, H.; Yamaguchi, D.; Hashimoto, T., Bacterium organizes hierarchical amorphous structure in microbial cellulose. *Eur. Phys. J. E* **2008**, *2*, 137-142.

(5) Glatter, Whittaker, J. L.; Balu, R.; Knott, R.; de Campo, L.; Mata, J. P.; Rehm, C.; Hill, A. J.; Dutta, N. K.; Roy Choudhury, N., Structural evolution of photocrosslinked silk fibroin and silk fibroin-based hybrid hydrogels: A small angle and ultra-small angle scattering investigation. *Int. J. Biol. Macromol.* **2018**, *114*, 998-1007.

(6) Mao, Y.; Liu, K.; Zhan, C.; Geng, L.; Chu, B.; Hsiao, B. S., Characterization of nanocellulose using small-angle neutron, X-ray, and dynamic light scattering techniques. *J. Phys. Chem. B* **2017,** *121*, 1340-1351.

(7) Pedersen, J. S.; Schurtenberger, P., Scattering functions of semiflexible polymers with and without excluded volume effects. *Macromolecules* **1996,** *29*, 7602-7612.